

AD-A068 448

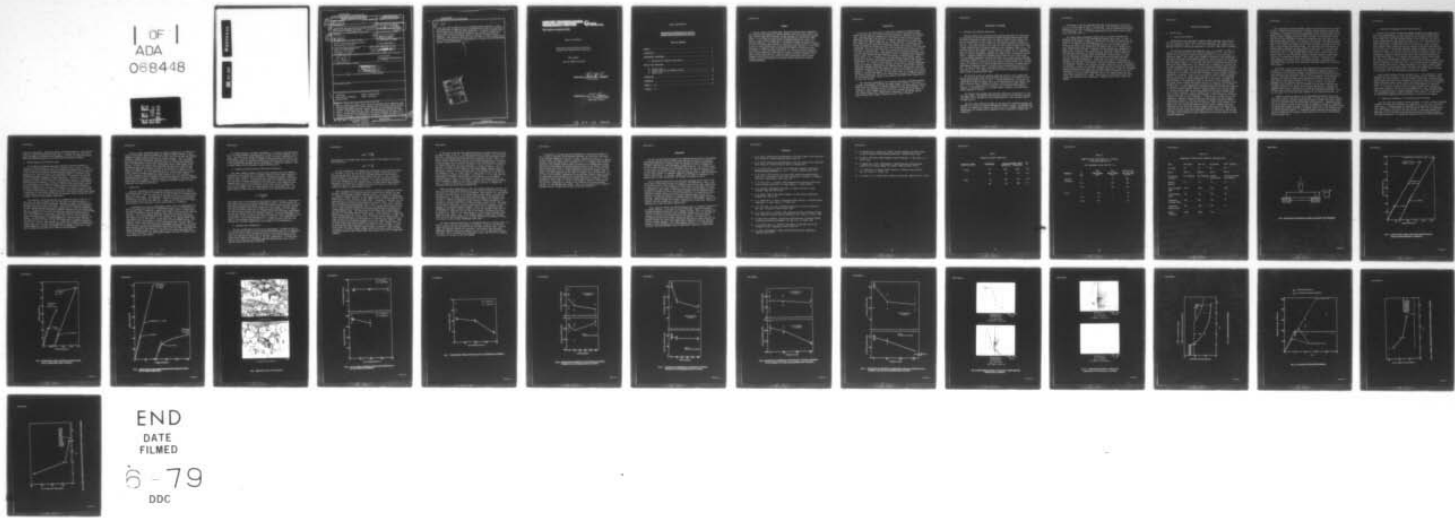
UNITED TECHNOLOGIES RESEARCH CENTER EAST HARTFORD CONN
FABRICATION AND EVALUATION OF LOW COST ALUMINA FIBER REINFORCED--ETC(U)
JAN 79 K M PREWO
N00014-76-C-0035

NL

UNCLASSIFIED

UTRC/R79-912245-6

1 OF
ADA
068448



END
DATE
FILED
0 - 79
DDC

DDC FILE COPY

AD A068448

UNCLASSIFIED

SECURITY CLASSIFICATION OF THIS PAGE (When Data Entered)

REPORT DOCUMENTATION PAGE			READ INSTRUCTIONS BEFORE COMPLETING FORM
1. REPORT NUMBER UTRC R79-912245-6	2. GOVT ACCESSION NO.	3. RECIPIENT'S CATALOG NUMBER	
4. TITLE (and Subtitle) FABRICATION AND EVALUATION OF LOW COST ALUMINA FIBER REINFORCED METAL MATRICES		5. TYPE OF REPORT & PERIOD COVERED Final Technical Report 1 Jul 1975 - 30 Nov 1978	
6. AUTHOR(s) Karl M. Prewo		7. CONTRACT OR GRANT NUMBER(S) N00014-76-C-0035	
8. PERFORMING ORGANIZATION NAME AND ADDRESS United Technologies Research Center East Hartford, CT 06108		9. PROGRAM ELEMENT, PROJECT, TASK AREA & WORK UNIT NUMBERS NR 031-7849-23-77	
10. CONTROLLING OFFICE NAME AND ADDRESS Office of Naval Research Department of the Navy Arlington, VA 22217		11. REPORT DATE Jan 1979	
12. NUMBER OF PAGES 36		13. SECURITY CLASS. (of this report) Unclassified	
14. MONITORING AGENCY NAME & ADDRESS (if different from Controlling Office) 44-P.		15a. DECLASSIFICATION/DOWNGRADING SCHEDULE	
16. DISTRIBUTION STATEMENT (of this Report) DISTRIBUTION STATEMENT A Approved for public release; Distribution Unlimited			
17. DISTRIBUTION STATEMENT (of the abstract entered in Block 20, if different from Report)			
18. SUPPLEMENTARY NOTES			
19. KEY WORDS (Continue on reverse side if necessary and identify by block number) Composites Metal matrix composites Alumina fiber Silicon carbide fiber Impact tolerance			
20. ABSTRACT (Continue on reverse side if necessary and identify by block number) Silicon carbide and alumina fiber reinforced aluminum matrix composites were evaluated and compared by tensile testing, three point bend flexural testing, elevated temperature exposure, thermal cycling, and instrumented pendulum impact. It was found that the silicon carbide/aluminum provided the higher level of axial tensile strength while the alumina/aluminum was superior in transverse tension. The difference in transverse strength was mainly due to the poor fiber-matrix bond existent in the silicon carbide/aluminum as compared			

449252

UNCLASSIFIED

SECURITY CLASSIFICATION OF THIS PAGE(When Data Entered)

20. Cont'd

to the very high strength bond in the alumina/aluminum composite. A very large difference in composite impact performance was found to be affected by the differences in fiber and matrix properties. In addition, measured composite impact energy dissipation capability was related to specimen test geometry as well as the relative levels of composite tensile and shear strengths. Both composite materials were also shown to suffer significantly due to either thermal cycling (SiC/aluminum) or constant elevated temperature exposure (alumina/aluminum).

ACCESSION for

NTIS	White Section	<input type="checkbox"/>
DOC	Buff Section	<input type="checkbox"/>
UNANNOUNCED		
JUSTIFICATION		
Per HR. on File		
BY		
DISTRIBUTION/AVAILABILITY CODES		
or SPECIAL		
A		-

UNCLASSIFIED

SECURITY CLASSIFICATION OF THIS PAGE(When Data Entered)

UNITED TECHNOLOGIES RESEARCH CENTER



East Hartford, Connecticut 06108

Report R79-912245-6

Fabrication and Evaluation of Low Cost Alumina Fiber Reinforced Metal Matrices

FINAL REPORT

Contract N00014-76-C-0035

REPORTED BY

Karl M. Prewo
K. M. Prewo

APPROVED BY

E. R. Thompson
E. R. Thompson, Manager
Materials Sciences

79 04 02 022

Fabrication and Evaluation of Low Cost
Alumina Fiber Reinforced Metal Matrices

TABLE OF CONTENTS

SUMMARY	1
INTRODUCTION	2
EXPERIMENTAL PROCEDURES	3
A. Materials and Composite Fabrication	3
RESULTS AND DISCUSSION	5
A. Tensile Test	5
B. Thermal Exposure and Thermal Cycling	8
C. Impact Test	9
CONCLUSIONS	14
REFERENCES	15
TABLES I - III	17
FIGURES 1 - 17	

SUMMARY

Silicon carbide and alumina fiber reinforced aluminum matrix composites were evaluated and compared by tensile testing, three point bend flexural testing, elevated temperature exposure, thermal cycling, and instrumented pendulum impact. It was found that the silicon carbide/aluminum provided the higher level of axial tensile strength while the alumina/aluminum was superior in transverse tension. The difference in transverse strength was mainly due to the poor fiber-matrix bond existent in the silicon carbide/aluminum as compared to the very high strength bond in the alumina/aluminum composite. A very large difference in composite impact performance was found to be affected by the differences in fiber and matrix properties. In addition, measured composite impact energy dissipation capability was related to specimen test geometry as well as the relative levels of composite tensile and shear strengths. Both composite materials were also shown to suffer significantly due to either thermal cycling (SiC/aluminum) or constant elevated temperature exposure (alumina/aluminum).

INTRODUCTION

In the past, the application of metal matrix composite systems has been hampered by the high cost of these materials relative to resin matrix composites. Although aluminum, magnesium and titanium matrix composites have offered significant advantages, the high cost of the initial fiber, which has principally been boron, and the high cost of composite fabrication by hot pressing have combined to inhibit widespread use. Recent progress in both fiber technology and composite fabrication procedures, however, have provided new avenues to overcome this cost barrier and still retain major metal matrix composite advantages. Three new continuous fibers have opened the possibility to achieving true low cost reinforcement. These are an alpha alumina yarn, called fiber FP, a silicon carbide yarn, and a large diameter silicon carbide monofilament. All three of these fibers have been examined in detail to determine their characteristics (Refs. 1,2). In addition, the fabrication of aluminum matrix composites reinforced with each of these fibers was investigated using casting, powder metallurgical and hot press diffusion bonding of plasma sprayed tape techniques (Refs. 1,2). As a result of these studies it was shown that the FP alumina reinforced aluminum, fabricated by casting, and the silicon carbide monofilament reinforced aluminum, fabricated by hot pressing plasma sprayed tapes, offered mechanical properties that were competitive with boron and graphite reinforced aluminum. In addition, the fabrication procedures used offered low cost alternatives to existent techniques. For this reason these two systems were selected for further evaluation. The silicon carbide yarn reinforced aluminum composite was not pursued further because of its inferior performance when compared with the other two systems.

The following investigation into composite performance emphasized material strength, environmental stability and impact damage tolerance. All three of these areas are important in composite application, with environmental stability being one of the important areas of preference for metal matrix systems. The last topic, impact damage tolerance, is also of extreme importance because of the possible application of metal matrix composites in gas turbine engines where foreign object damage tolerance has been a major inhibitor.

EXPERIMENTAL PROCEDURES

A. Materials and Composite Fabrication

Silicon carbide fiber reinforced 6061 aluminum composites were fabricated by the process of solid state diffusion bonding together plasma sprayed tapes. The fiber, purchased from Avco Corp., was 140μ in diameter with a carbon core, and was obtained with a spool strength of 3400 MPa and an elastic modulus of 415 GPa. This fiber was wound onto a 25μ thick 6061 aluminum foil covered mandrel at a controlled spacing of 128 turns per inch and then covered with a layer of 6061 aluminum powder by plasma spraying in inert atmosphere (Refs. 2,3). The resultant tape is then removed from the mandrel and easily cut into individual plies for stack up and bonding. Because this tape consists only of aluminum and fiber, no further outgassing treatments are required prior to composite consolidation. Composite bonding was performed with the matrix in the solid state, i.e. the maximum temperature was below the 6061 alloy solidus and the resultant composites contained 45% by volume of SiC fiber. The bonding procedure, referred to as "Quick Bond" is described in greater detail elsewhere (Refs. 2,4). Briefly stated, it consisted of hot pressing together multiple layers of plasma sprayed tape between preheated platens, in vacuum, using an applied pressure of 34.5 MPa. The total process time, including evacuation of the bonding chamber, is less than 30 min. Test samples were then cut from the resultant hot pressed panels using a diamond abrasive wheel.

The FP fiber reinforced aluminum composites tested in this program were all cut from a single large unidirectionally reinforced plate obtained from the Pioneering Research Division of the E. I. DuPont DeNemours Co. The plate contained 60% by volume of alumina fiber in an aluminum-lithium alloy matrix. The fiber, given the name FP alumina by DuPont, is described in greater detail in Ref. 1. It is in continuous yarn form with each individual fiber having a diameter of approximately 20μ , an average tensile strength of 1720 MPa and an elastic modulus of 345 GPa.

All tensile test specimens were parallel sided, flat coupons with a 2.5 cm long gage length. Fiberglass reinforced epoxy doublers were bonded to the gripping areas of each specimen and strain gages applied to both specimen sides in the gage section.

The three point flexural strength of both axial and transverse specimens was measured as a function of thermal exposure and thermal cycling. The maximum temperature of exposure was chosen to be 370°C , since it is highly unlikely that any applications for aluminum matrix composites will be permitted to exceed this temperature.

The thermal cycles were performed with heat up occurring over a period of 4 min in a furnace held at 370°C. An additional 4 min residence time was then followed by a cool down in ambient air for 4 min, with the specimen reaching 25°C in approximately 2 min. All flexure specimens were tested with a span-to-depth ratio of at least 40 to 1.

The impact energy dissipation capabilities of composite specimens was measured through the use of the instrumented pendulum impact test. In this procedure the specimen is loaded in a three point bend mode and impacted at the center of its span with an instrumented striker, or tup traveling at a speed of 3 meters per second. The tup is instrumented by the use of strain gages so that, through appropriate calibration, the applied load vs time history of an impact event can be recorded. A schematic of the specimen test arrangement is shown in Fig. 1 where it can be seen that, for the herein reported data, the specimens were unnotched, the overall specimen test span is held constant at 4.0 cm, and both the specimen depth (h) and width (b) were varied. In every case the specimens were uniaxially reinforced with the principal fiber axis parallel to the span dimension L. In the case of the SiC reinforced 6061 aluminum, two different specimen orientations, with respect to the planes of the individual tape plies, were tested. The two orientations, termed "chordwise" and "edgewise", relate to the direction of impact relative to the ply orientation. As described previously, the SiC/6061 specimens have been fabricated by diffusion bonding together monolayer tape plies of plasma sprayed tape. Thus, the "chordwise" orientation refers to an impact where the tup strikes the composite in a direction normal to the plies while "edgewise" refers to an impact wherein the tup strikes the composite plies on edge. These terms are synonymous with the terminology used to describe the orientation of impacts on gas turbine engine fan blades.

RESULTS AND DISCUSSION

A. Tensile Test

1. Stress Strain Behavior

Longitudinally and transversely oriented tensile specimens were tested at 22°C for both the SiC and FP fiber reinforced composites. The stress strain data are presented in Figs. 2-4. For the SiC reinforced 6061 composite, specimens were tested in both the as-fabricated (F) and heat treated (T-6) conditions.

The SiC/6061 longitudinal specimen data, Fig. 2, are similar to those obtained in the past for boron fiber reinforced aluminum (Ref. 5). The curve is made up of two essentially linear portions separated by a small non-linear transition region. The initial linear segment corresponds to that during which both matrix and fiber are deforming elastically. Hence the slope of this segment can be obtained from a rule of mixtures calculation based on the constituent material elastic moduli. In the current case these are 68.9 GPa and 415 GPa for matrix and fiber respectively. The average value of composite E_{11} obtained for all tests performed was 211 GPa which is in reasonable agreement with a value of 220 GPa calculated on the basis of the above values and a known composite fiber content of 45% by volume. The secondary "elastic" modulus indicated in Fig. 2 corresponds to the region in which fiber deformation is still elastic and matrix deformation is plastic. Thus, the value of modulus obtained should be approximated by the sum of the elastic fiber contribution and a term that represents the contribution due to the work-hardening rate of the matrix. Although this region appears to be essentially linear in the figure, closer examination of the actual curves revealed some gradual decrease in slope with increasing stress probably due to a continuing decrease in matrix work hardening rate as strain is increased. The only significant difference between the stress-strain behavior of the T-6 condition material and the F condition material was that the region of transition from primary to secondary modulus was much more extended in the case of the T-6 material. This is probably due to an increase in 6061 matrix yield strength (the T-6 condition yield strength of 6061 aluminum is 145 MPa as compared to 55 MPa for the F condition). It should also be noted that in both conditions, composite ultimate failure took place without any major change in stress-strain behavior. The only indication of imminent failure was several small "jogs" in the curve just prior to fracture. This is also similar to the behavior of boron reinforced aluminum where, by acoustic emission and X-ray techniques, it was found that overall composite failure occurred immediately after the fracture of the first high strength fibers (Refs. 6,7). Only in the presence of large imposed stress gradients, such as are present in the vicinity of notches, was it possible to get a sequential fiber fracture pattern for high strength composites.

The transversely oriented SiC/6061 composite stress-strain curves are shown in Fig. 3, where it can be noted that the effect of heat treatment is much more pronounced. In this case the T-6 heat treatment caused a major increase in composite tensile strength, as would be expected due to the increase in 6061 matrix ultimate tensile strength of from 125 MPa to 310 MPa. It is important to note that in both cases the observed composite strength was well below that of the unreinforced matrix strength. This is due to the fact that the composite failure mode was predominantly through the fiber-matrix interface. As noted previously, (Ref. 2) the carbon rich surface layer of the SiC filaments prevents the attainment of high strength fiber-matrix bonds. The transverse tensile properties of aluminum matrix composites has been examined in great detail in the past, both analytically (Refs. 8,9) and experimentally (Refs. 5,10). It has been found that in the case of a high strength fiber-matrix interface, which causes composite failure to occur through the matrix, composite strength is nearly equal to that of the unreinforced matrix regardless of percent fiber content. For other cases, however, where either interfacial failure or transverse fiber splitting modes of failure occur, the composite strength is expected to be considerably less than that of the matrix and decreases rapidly with increasing fiber content.

The stress vs strain curves for both longitudinal and transverse tensile specimens of FP alumina fiber reinforced aluminum are presented in Fig. 4. As in the case of the SiC/6061 specimens, the longitudinal specimen behavior is characterized by two essentially linear regions with initial matrix yield occurring at a relatively low level of stress. By acid digestion it was possible to determine that these specimens contain approximately 60% by volume of fiber and, using a fiber elastic modulus of 345 GPa, it is possible to get good agreement with the measured composite E_{11} value of 226 GPa. The value of secondary elastic modulus is also in agreement with the almost complete loss of matrix contribution to modulus due to plastic deformation. The major differences between the FP alumina and SiC reinforced longitudinal specimens is the much lower strength and failure strain of the FP reinforced material. This is, of course, due to the much lower strength of the alumina fibers (Ref. 1).

Composite transverse behavior of the FP/aluminum specimens, Fig. 4, was also found to differ from that of the SiC/6061. In this case the alumina fiber reinforced specimens exhibited significantly higher strengths and failure strains due to the excellent bond achieved between fiber and matrix. Composite fracture occurred primarily through the matrix with no evidence of interfacial debonding. The rather large degree of plastic deformation exhibited by these specimens is also of considerable significance and is in marked contrast to the low failure strain of the SiC/aluminum material. A comparison between composite and unreinforced matrix strengths was not possible at this time due to the lack of unreinforced matrix strength data.

2. Specimen Fractography and Fiber-Matrix Bonding

The SiC and FP alumina reinforced aluminum systems differ dramatically in their fracture appearance. As described above, the FP fiber-aluminum matrix bond is extremely strong while that between SiC and aluminum is much weaker. In the former case, the high strength bonding is due to the fact that the FP fiber is readily wet by, and reacts with, the Al + Li alloy matrix during composite fabrication by liquid metal infiltration (Ref. 1). A thin SiO_2 rich fiber surface layer is penetrated by the Li of the molten matrix to produce a lithia-alumina spinel product and also an extremely strong fiber-matrix bond. Thus, in the case of FP/aluminum transverse tensile specimens, fracture occurred through the matrix. In the case of the SiC reinforced aluminum, however, the fiber has a carbon rich surface layer which prevents fiber-matrix reaction and bonding when composite fabrication takes place with the matrix maintained in the solid state (Ref. 2). As a result, the transverse tensile fracture mode was found to be predominantly through the fiber-matrix interface. It should be noted that this is in marked contrast to a SiC coated boron fiber-matrix bond condition studied in the past (Ref. 11). The bond between Borsic filaments and 6061 aluminum, fabricated in a manner analogous to the present SiC/6061 composites, was found to be extremely strong and caused those composites to exhibit an all matrix transverse failure mode. In that case, however, the SiC coating was not carbon rich, and fiber-matrix bonding was not impeded.

Axial tensile specimen fracture surfaces, Fig. 5, also reflected the above fiber-matrix bond situations as well as the influence of fiber diameter, fiber strength, and matrix strength. If both composite systems were characterized by high strength fiber-matrix bond situations, the pullout length of the FP/aluminum system (calculated using a simple "shear lag" expression) would be only approximately 60μ while that for the SiC/6061 would be approximately 30 times that value. It is expected, however, that the contrast between these systems is even larger because of the very poor SiC-aluminum bond. Thus, the FP/aluminum tensile fracture surface is almost completely free of any fiber protrusion while the SiC/aluminum composite exhibited extensive fiber pullout. In both cases the aluminum surrounding the fibers deformed in a locally ductile manner.

3. Temperature Dependence of SiC/Aluminum Tensile Strength

Both the axial and transverse tensile strengths of the SiC reinforced aluminum composite decreased with increasing test temperature. In the case of the axial tests, Fig. 6, a slight decrease in strength was observed with an increase in test temperature to 200°C while the data obtained at 375°C are not reported because all fractures occurred in the grip area due to excessive clamping force. This high force was required since the entire specimen, including the grips, was heated during test. No significant decrease in primary elastic modulus was

noted with temperature. Transverse tensile strength decreased to a much greater extent over the same temperature range, Fig. 7. Despite the major decrease in matrix strength by raising the test temperature to 375°C, the composite failure mode still remained primarily one of fiber-matrix interfacial failure.

B. Thermal Exposure and Thermal Cycling

The retention of composite axial and transverse flexural strength as a function of time exposed to air at 370°C is shown in Figs. 8 and 9. In both orientations the SiC reinforced 6061 was unaffected by exposure while in the case of the FP reinforced aluminum, strength decreased dramatically with increasing exposure time. This was due to a very noticeable degree of oxidation of the FP/aluminum composite surfaces which turned black, as compared to the SiC/6061 which was generally unchanged in overall appearance. The surface residue was examined by removal and collection for X-ray analysis; however, no unambiguous identification was possible. At best, it appeared that there was some evidence for the presence of an aluminum silicate, along with the very obvious aluminum and alpha alumina fiber. The very large decrease in FP/aluminum transverse flexural strength may also be due to a softening of the matrix since the depth of surface oxidation was not sufficient to reduce the observed strength by 50%. In addition, the transverse specimens failed in a relatively ductile (large degree of bend) manner, both in the as-received and thermally exposed conditions, indicating no selective embrittlement taking place.

The thermally cycled specimen data are presented in Figs. 10 and 11. In this case, the axial strength of the SiC reinforced aluminum decreased to a greater extent than did the FP/aluminum, although once again the oxidation of the latter system was readily noticeable. This marked decrease was accompanied by some specimen warpage which was most apparent for the transverse specimens, Fig. 11. In general, the FP/aluminum specimens exhibited far less warpage than the SiC/aluminum. This is due to the important differences between these systems. First, the difference in coefficient of thermal expansion between fiber and matrix is slightly less for the FP/aluminum than it is for the SiC/aluminum system. The coefficients of thermal expansion of aluminum, alpha alumina, and SiC fiber are 23.8, 5.7 and $4.4 \times 10^{-6}/^{\circ}\text{C}$ respectively. Secondly, the much smaller size of the FP fiber provides for a much more homogeneous distribution of materials, and hence less likely imbalance in overall material coefficient of thermal expansion. As such, the tendency for a specimen to warp out of plane due to thermal cycling would be far less for the FP/aluminum.

Finally, another interesting aspect of composite behavior is to compare the values of three point flexural strength and tensile strength obtained. A data comparison is made in Table I where it can be seen that in every case the flexural strength is significantly greater than the tensile strength. This is in agreement with other fiber reinforced composites (Ref. 12) where it has been shown that a rationalization of this effect can be based on a statistical analysis of failure. In brief, the tensile test configuration places a much larger volume of material under high tensile stress than does the three point flexural test. Thus, the probability for failure, caused by the presence of a defect in this volume, is enhanced. The exact magnitude of the F/T ratio is dependent on the actual composite strength population distribution, with materials characterized by a wider spread in data exhibiting larger values of F/T. This analysis, although providing excellent agreement for monolithic materials such as ceramics, is more difficult to apply to composites where the possibility of multiple failure modes (shear and compression as well as tension) in flexural testing can cause deviations from expected performance.

C. Impact Test

The test configuration used for impact testing is shown in Fig. 1 and the instrumented impact traces for SiC/6061 and FP/aluminum specimens are shown in Figs. 12 and 13. In each case the load on the tup is shown as a function of time during the impact event. The specimens of SiC/6061 were tested in two different orientations, "chordwise" and "edgewise". These two terms are described above and have been used in the past (Ref. 13) to refer to the direction of the impact event relative to the tape plies of fiber reinforcement in a composite.

A comparison of the load vs displacement traces, Fig. 12, demonstrates that there is a significant difference in performance between the two orientations. The chordwise impact dissipates a significantly greater amount of energy due to extensive interlaminar shear deformation, which takes place between the composite tape plies. Due to the somewhat inadequate fiber-matrix bonding existent in this system, the vestigial remnants of the original planar fiber arrays permit interlaminar shear to take place. On the other hand, the edgewise impact event required a nearly 15% increase in applied load to cause specimen failure. The composite failure mode consisted of less interlaminar shear and more tensile fiber fracture. In both the chordwise and edgewise impacts, however, the specimens deformed extensively and dissipated large levels of energy. The amount of energy dissipated is very similar to that typical of boron fiber reinforced 6061 aluminum specimens tested in a manner similar to that herein described (Refs. 13,14) where the fiber is the same nominal diameter and tensile strength as the fiber described in this report.

In extreme contrast, the impact performance of a similarly configured specimen of FP fiber/aluminum is characteristic of that of a brittle material, Fig. 13 (top). The total impact energy dissipated is only 5% of that characteristic of SiC/aluminum. There are two major reasons for this difference; the first is due to major differences in composite microstructure while the second reason relates to the specimen test geometry and its relationship to composite properties. Each of these reasons will be discussed in greater detail below.

1. Composite Microstructure and Fiber-Matrix Properties

The impact damage tolerance of metal matrix composites has been examined extensively in the recent past to determine methods by which impact energy dissipation can be optimized for the purposes of improving structural component survival (Refs. 13-16). In the case of boron reinforced aluminum, it was shown that the amount of energy dissipated during impact (in a three point bend configuration such as the one used herein) can be related to the composite parameters of fiber diameter (d_f), effective in-situ fiber tensile strength (σ_f), matrix shear strength (τ_m), and volume percent fiber reinforcement (V_f). The impact energy (E) was found to be proportional to the expression given below.

$$E \propto \frac{V_f d_f \sigma_f^2}{\tau_m}$$

This formula was first developed to help describe the performance of composites in which fiber pullout is an important mechanism of failure. As shown herein and previously, this mechanism applies to the SiC/aluminum system and would also imply that the FP/aluminum system would dissipate far less energy. Using this expression and the material properties of fiber and matrix described in this report, the above equation predicts that the SiC/6061 system would dissipate approximately 40 times more energy than the FP/aluminum composite. By actual measurement, the data in Figs. 12 and 13 indicate this ratio is between 20 and 30, depending on the orientation of the SiC/6061 specimen used for comparison. This comparison was made for the specimens tested with $L/h = 4$. As will be shown below, the comparison will be altered significantly with changes in test configuration.

2. Specimen Test Configuration

The test configuration used is also of significance. As shown in Fig. 13, the load-deflection trace for the FP reinforced aluminum appears to be completely free of any sign of plastic deformation after initial fracture when a particularly thin specimen is tested, Fig. 13 (bottom). This can be related to the stress state caused by the geometry of the test configuration. In three point bend it can be shown that the maximum applied flexural stress occurs at the specimen tensile surface and is given by:

$$\sigma_{\max} = 3/2 \frac{PL}{bh^2}$$

Simultaneously, the maximum shear stress is caused at the midplane of the specimen and given by:

$$\tau_{\max} = 3/4 \frac{P}{bh}$$

In these expressions P represents the load applied to the specimen midspan, L is the span, b and h are the specimen width and depth respectively, Fig. 1. Thus, during any given test the ratio of maximum applied shear and flexural stresses depends on the specimen span-to-depth ratio (L/h). Since a given material can fail by either shear or tension, one of these failure modes will occur first depending on test configuration. For high longitudinal strength composites, the large ratio of tensile to shear strength causes these materials to deform by shear for test configurations having low values of (L/h) and to fracture in tension for high values of (L/h).

Thus, for small values of (L/h) it would be possible to accurately determine the shear strength of the composite material using the above formula for τ_{\max} . As long as all specimens initially deformed by shear, the calculated value of τ_{\max} would be constant and equal to the composite shear strength τ_0 , independent of the value of (L/h). However, at some higher value of (L/h) the material would eventually fail in flexure on the tension side. An attempt to calculate the true shear strength at this point would produce an inaccurate value. This is shown, both by calculation and experimental data in Fig. 14. In this figure, referred to as a "shear interaction diagram", (Ref. 17) the maximum shear stress was calculated using the above formula and the maximum applied impact load taken from the instrumented traces. The data points in the figure were obtained experimentally. If only these data points were used, it would appear that composite shear strength varies with (L/h). This, however, is not the case. At high (L/h) values the specimens fail in flexure due to the high surface tensile stress. The drawn curves in the figure are not placed to fit the data, but instead are calculations based on the flexural strength (σ_0) of the composite, Table I. Thus, for (L/h) values less than 12, SiC/6061 is expected to fail in shear, while for FP/aluminum shear controlled failure only occurs for (L/h) less than 4. Below these values the actual composite shear strength is obtained. There is more uncertainty in the matrix shear strength of the Al/Li alloy, however, the 6061 aluminum matrix has a well defined value which agrees with that for wrought 6061 aluminum.

It should be noted that this analysis resolves a noticeable difficulty with the data of Figs. 12 and 13. In these load-deflection traces it can be noticed that the 1 cm square cross section specimens of SiC/6061 and FP/aluminum require nearly the same maximum applied load to cause composite fracture. This is in direct conflict with the fact that the SiC reinforced material has been shown to be much stronger, both in tension and flexure, than the FP/aluminum. Using Fig. 14, however, this point can now be resolved. At an L/h value of 4, the former material is failing in shear while the later is failing in flexure. This is shown more clearly in Fig. 15 where the calculated maximum flexural stress is plotted as a function of span-to-depth ratio. This diagram can be considered the companion to Fig. 14 in that, only for large values of L/h is the true composite flexural strength (σ_0) obtained. At an (L/h) of 4, it is clear that the SiC/aluminum is failing in shear while the FP/aluminum is at its maximum flexural strength. Thus, it is necessary to report the composite data in the form of measured strength vs L/h to get a complete picture of composite performance. It should be noted that the sloping lines in the low L/h regions are calculated based on matrix shear strength data.

There are other consequences of this test geometry dependence as well. In Fig. 16 the measured energy dissipated per unit cross sectional area of specimen is plotted as a function of L/h for SiC/aluminum. This quantity is a very strong function of L/h and relates to the stress state induced change in failure mode discussed above. At values of L/h below 12, matrix shear is an important contributor to composite deformation and controls the maximum load achieved prior to failure. This is accompanied by large amounts of plastic deformation, in contrast to specimens which fail in flexure at higher values of L/h . Also shown in the figure is the value of elastic energy which would be required to raise a specimen to its maximum flexural strength. This value is obtained by simply integrating the elastic flexural stress field over the specimen volume and, for the purposes of comparison with the data in the figure, dividing by the cross sectional area. Thus, at very large values of L/h the energy dissipated nearly equals the fully elastic case. It is somewhat higher in actual fact because there are still shear stresses which can cause some matrix deformation, however, very little overall specimen deformation takes place.

The impact energy dissipated by the FP/aluminum material is shown in Fig. 17 where it can be seen that total degree of variation, as well as the absolute values obtained, are far less than for the SiC fiber reinforced case. Surprisingly, the agreement between the calculated fully elastic case and actual experiment appears rather poor; however, this is due to the high resolution of the scale. The actual magnitude of difference is less than 10 kJ/m^2 as compared to 30 kJ/m^2 in the case of the SiC/aluminum.

In addition to the above described dependence of specimen performance on L/h , a series of SiC/6061 and FP/aluminum specimens was tested with variations in the specimen dimension b (see Fig. 1) with a constant L/h value of 4. The resultant data, presented in Table II, indicate that for both systems the maximum fracture stress was unaffected by variations in b . In agreement with the above discussion, the SiC/6061 failure stress is presented as a maximum shear stress while for the FP/aluminum the maximum flexural stress was calculated. Specimen energy dissipation, however, varied significantly with change in b and in both cases the specimens with the largest dimension dissipated the highest levels of energy, even when normalized on the basis of specimen cross sectional area. In the case of the SiC/6061, examination of the specimens revealed a major increase in interlaminar shear deformation with increasing b while for the FP/aluminum specimens no major change in overall specimen appearance was detected. It is interesting to note that, for the SiC, this change in extent of shear deformation was not accompanied by a change in the condition for initial specimen failure, i.e. the maximum shear stress. Thus it is associated with a change in specimen fracture through crack growth and interply separation.

CONCLUSIONS

The data and discussion presented have demonstrated that both of the systems investigated possess properties which would make them attractive for selected engineering application. However, these two systems also differ significantly. A summary comparison of these composites is presented in Table III along with data for boron and graphite fiber reinforced 6061 aluminum. The SiC/6061 system is very similar in performance to Boron/6061 except for the very important aspect of fiber-matrix interfacial bonding. The very poor SiC fiber to aluminum bond causes a major penalty in composite transverse strength which in many applications would be prohibitive. In contrast, however, the SiC fiber is projected, by its manufacturer, to offer substantial cost savings as compared to boron.

The FP aluminum system has as its principal advantage the fact that a true liquid metal infiltration process can be used in its manufacture. Thus, it can be anticipated that a wide variety of shaped articles could be made economically. At present this is the only composite, of those listed in the table, which can be fabricated in this manner. Both boron and silicon carbide fibers are rapidly degraded in strength by contact with molten aluminum while the graphite fiber reinforced aluminum system is currently fabricated in a two stage process which requires the final consolidation of multiple aluminum-graphite wires by hot pressing. Significant penalties in composite density, impact damage tolerance, and axial tensile strength are, however, incurred with FP/aluminum. Thus, it is unlikely that this system will be able to substitute for boron fiber reinforced aluminum in any high performance applications.

Both composite systems also exhibited major losses of composite strength due to thermal exposure. In the case of the SiC/aluminum, composite transverse strength decreased significantly after thermal cycling. This is in marked contrast to the behavior of boron fiber reinforced aluminum (Ref. 18) and again is a result of the poor fiber-matrix bond in this system. The better bonded FP/aluminum system did not exhibit nearly the same level of sensitivity to thermal cycling, but instead was significantly degraded by simple constant temperature thermal exposure. Since metal matrix composites are often selected because of their insensitivity to environmental effects, it is expected that the above described phenomena would be significant inhibitors to application.

REFERENCES

1. K. M. Prewo, "Fabrication and Evaluation of Low Cost Alumina Fiber Reinforced Metal Matrices", Interim Technical Report, May 1977.
2. K. M. Prewo, "Fabrication and Evaluation of Low Cost Alumina Fiber Reinforced Metal Matrices", Interim Technical Report, November 1978.
3. K. G. Kreider and K. M. Prewo, "Boron Reinforced Aluminum", published in Metallic Matrix Composites, ed. by K. G. Kreider, Academic Press, 1974.
4. K. M. Prewo, "The Fabrication of Boron Fiber Reinforced Aluminum Matrix Composites", Proceedings of the First International Conference on Composite Materials, Geneva-Boston, AIME, April 1975.
5. K. M. Prewo and K. G. Kreider, "High Strength Boron and Borsic Fiber Reinforced Aluminum Composites", Jl. Comp. Matls., 1, (1972) 338-357.
6. H. W. Herring, "Fundamental Mechanisms of Tensile Fracture in Boron Aluminum", NASA-TR-R-383 (1972).
7. K. M. Prewo, "The Notched Tensile Behavior of Metal Matrix Composites", ASTM-STP-546, (1974), 507.
8. D. F. Adams and D. R. Doner, "Transverse Normal Loading of a Unidirectional Composite", Jl. Comp. Matls., 1, (1967), 152.
9. P. E. Chen and J. M. Lin, "Transverse Properties of Fibrous Composites", Mat. Res. & Standards, ASTM-9, August 1969.
10. K. M. Prewo and K. G. Kreider, "The Transverse Tensile Properties of Boron Fiber Reinforced Aluminum Matrix Composites", Met. Trans., 3, (1972), 2201.
11. K. Prewo and G. McCarthy, "Interfacial Characteristics of Silicon Carbide Coated Boron Reinforced Aluminum", Jl. Mat. Sci., 7, (1972), 919.
12. J. W. Hitchon and D. C. Phillips, "The Effect of Specimen Size on the Strength of cfrp", Composites, (April 1978) 119.
13. K. Prewo, "Development of Impact Resistant Metal Matrix Composites", AFML-TR-75-216 (1975).

14. D. McDanel and R. Signorelli, "Effect of Fiber Diameter and Matrix Alloys on Impact Resistant Boron-Aluminum Composites", NASA-TN-D-8204 (1976).
15. K. Prewo, "The Charpy Impact Energy of Boron Aluminum", J. Comp. Mats., 6, (1972), 442.
16. P. Melnyk and I. Toth, "Development of Impact Resistant Boron/Aluminum Composites for Turbojet Engine Fan Blades", NASA-CR-134770, (1975).
17. J. V. Mullin and A. Knoell, "Basic Concepts in Composite Beam Testing", Mat. Res. Stds., 12, (1970), 16.
18. K. Kreider, et al, "Metal Matrix Composite Technology", AFML-TR-71-204, (1971).

Table I
Composite Strength Comparison

<u>Composite System</u>	<u>Orientation</u>	<u>Average Strength (MPa)</u>		<u>F/T</u>
		Tensile(T)	Flexural(F)	
SiC/Al	0°	1490	2030	1.36
	90°	89	193	2.17
FP/Al	0°	590	860	1.46
	90°	222	380	1.7

Table II
Composite Impact Performance as a Function
of Specimen Dimension (b)
(all specimens tested with L/h = 4)

<u>Material</u>	<u>b</u> (cm)	<u>Max.</u> <u>Flex Stress</u> MPa	<u>Max.</u> <u>Shear Stress</u> MPa	<u>Impact Energy</u> <u>per Unit Area</u> (kJ/m ²)
SiC/6061 (edgewise)	1	-	95	600
	0.5	-	105	250
	0.25	-	110	225
FP/Al	1	750	-	28
	0.5	775	-	45
	0.25	775	-	42

Table III
Comparison of Metal Matrix Composite Characteristics

Fiber	140 μ Boron	140 μ SiC	FP Alumina	GY-70 Graphite
v/o Fiber	50	45	60	30
Matrix	6061-F	6061-F	Al-Li	6061-F
Fabrication Procedure	Hot Pressing	Hot Pressing	Casting Infiltration	Infiltration plus Hot Pressing
Density (gm/cm ³)	2.7	2.9	3.4	2.5
Axial Strength (MPa)	1400	1490	590	480
Axial Modulus (GPa)	235	210	225	207
Transverse Strength (MPa)	140	89	220	55
Transverse Modulus (GPa)	140	150	150	35
Impact Tolerance	High	High	Low	-

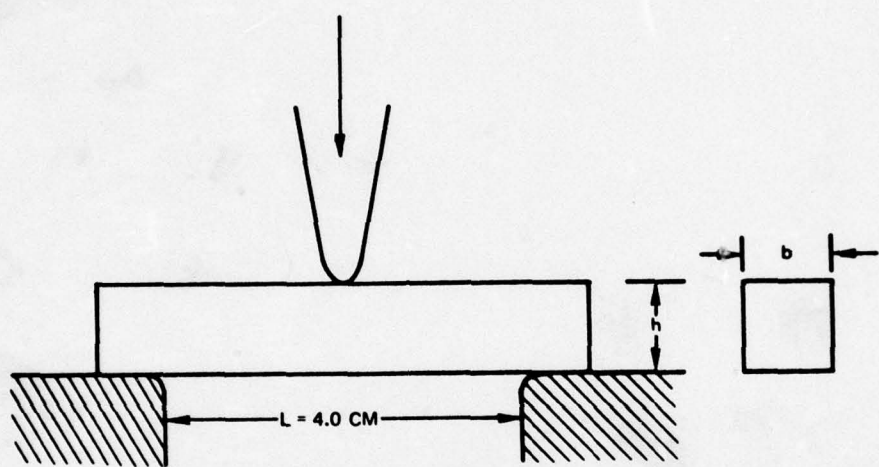


FIG. 1 UNNOTCHED INSTRUMENTED PENDULUM IMPACT TEST SPECIMEN

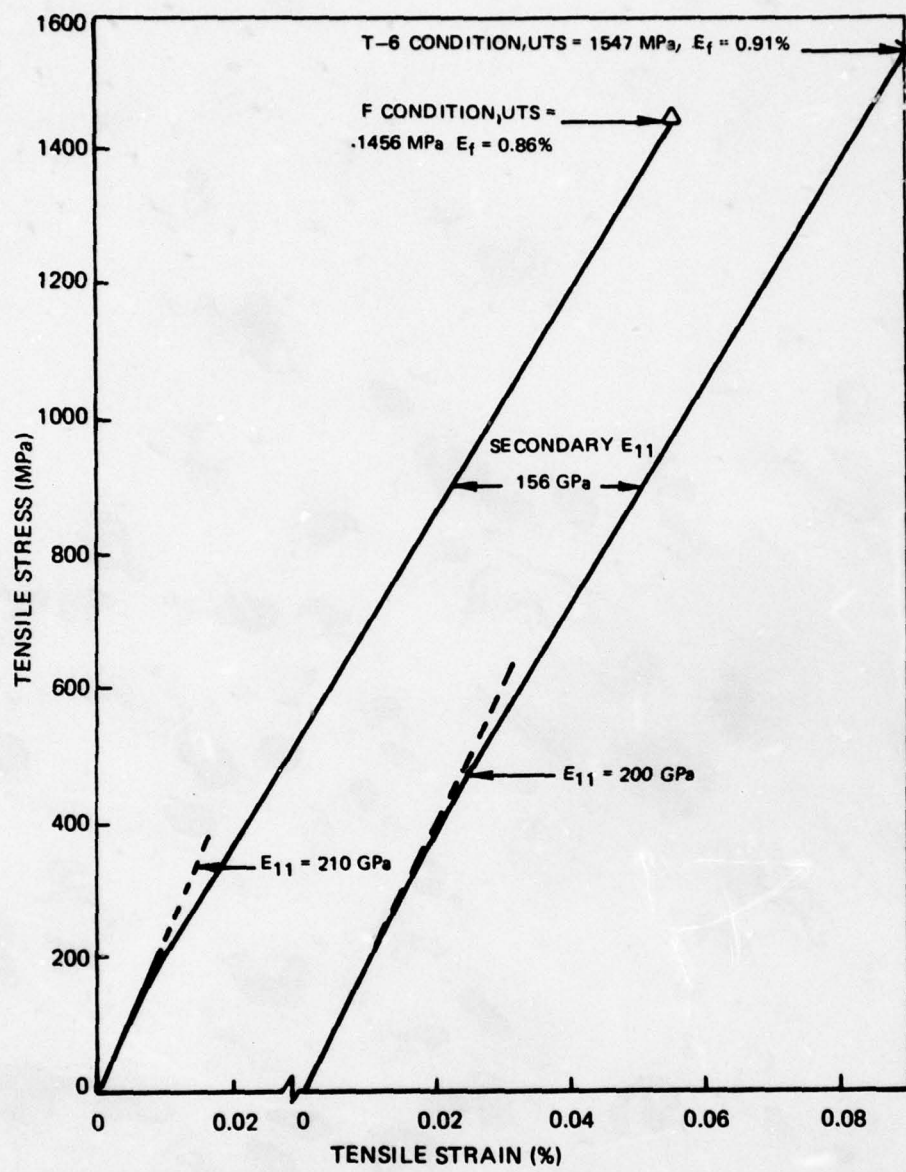


FIG. 2 LONGITUDINAL TENSILE STRESS VS STRAIN CURVES
FOR SiC REINFORCED 6061 ALUMINUM

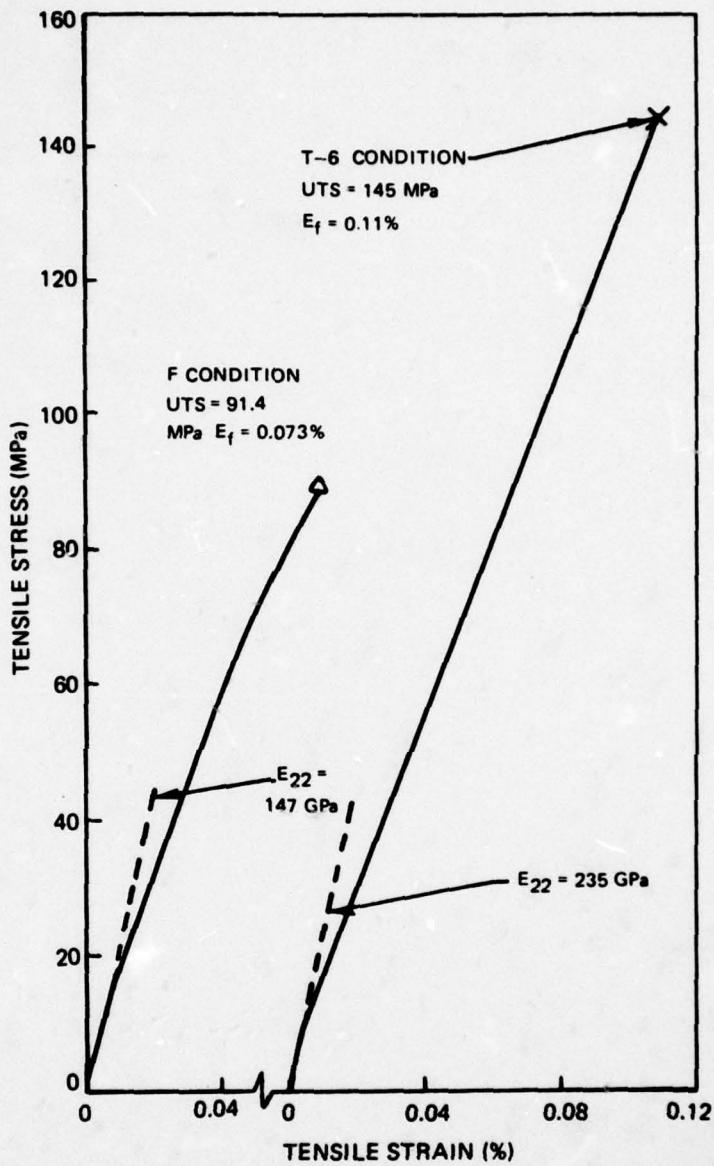


FIG. 3 TRANSVERSE TENSILE STRESS VS STRAIN CURVES
FOR SIC REINFORCED 6061 ALUMINUM

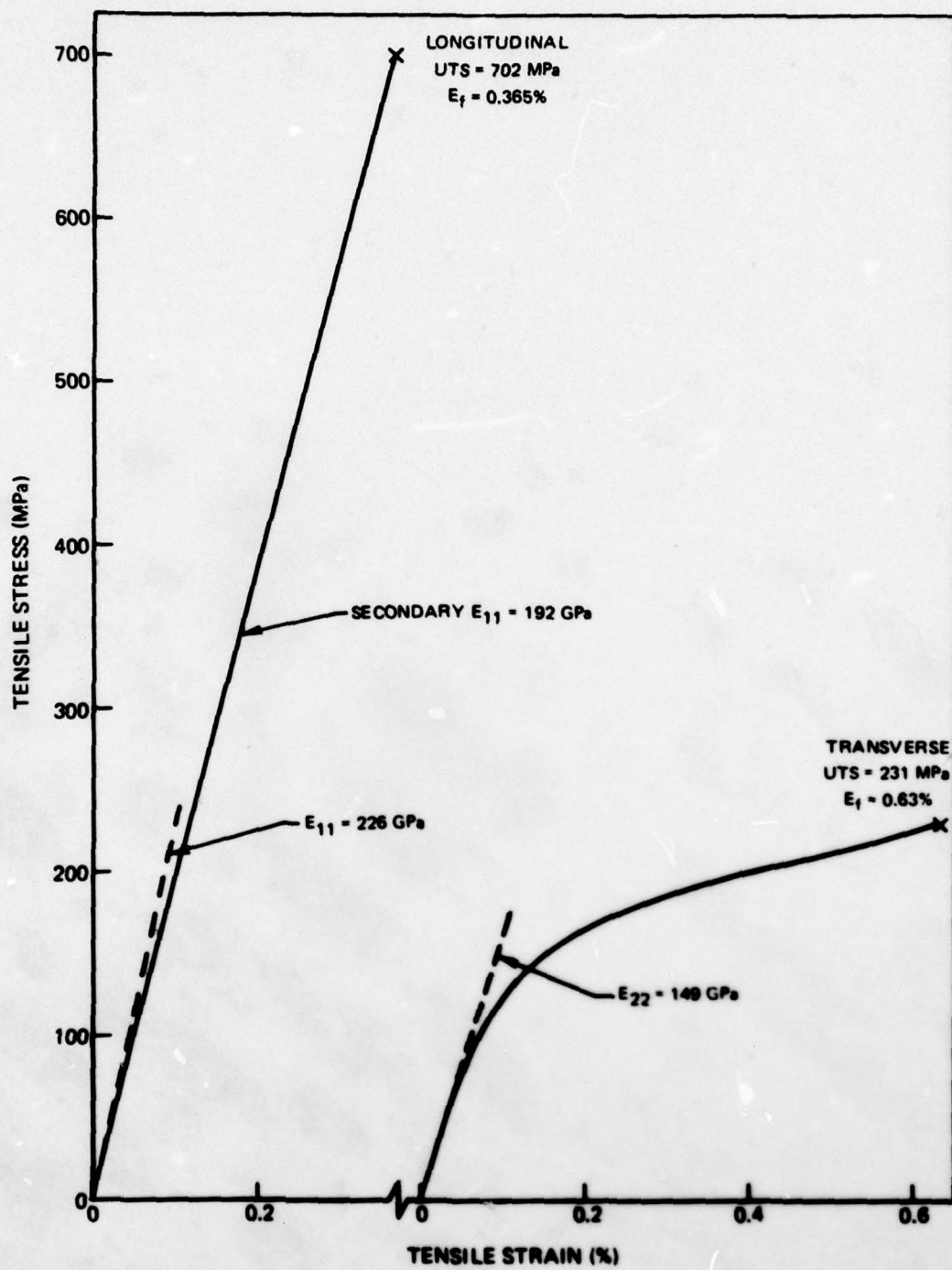
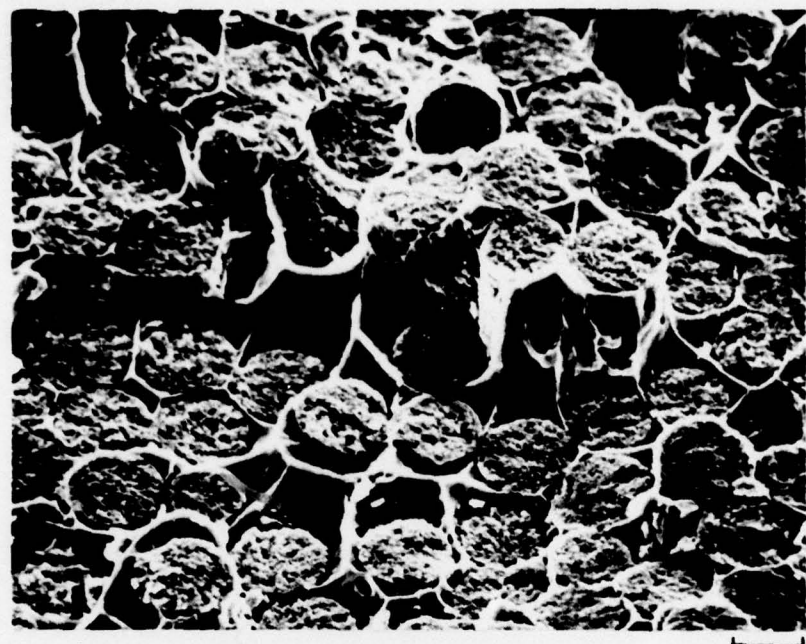
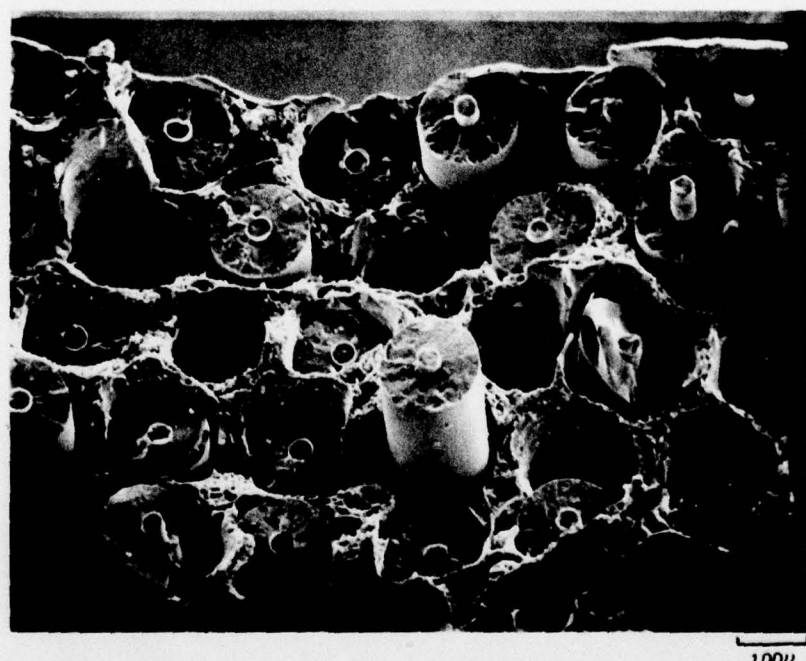


FIG. 4 LONGITUDINAL AND TRANSVERSE STRESS VS STRAIN CURVES
FOR FP FIBER REINFORCED



FP FIBER/ALUMINUM

20 μ



SiC MONOFILAMENT/ALUMINUM

100 μ

FIG. 5 SPECIMEN FRACTURE SURFACES

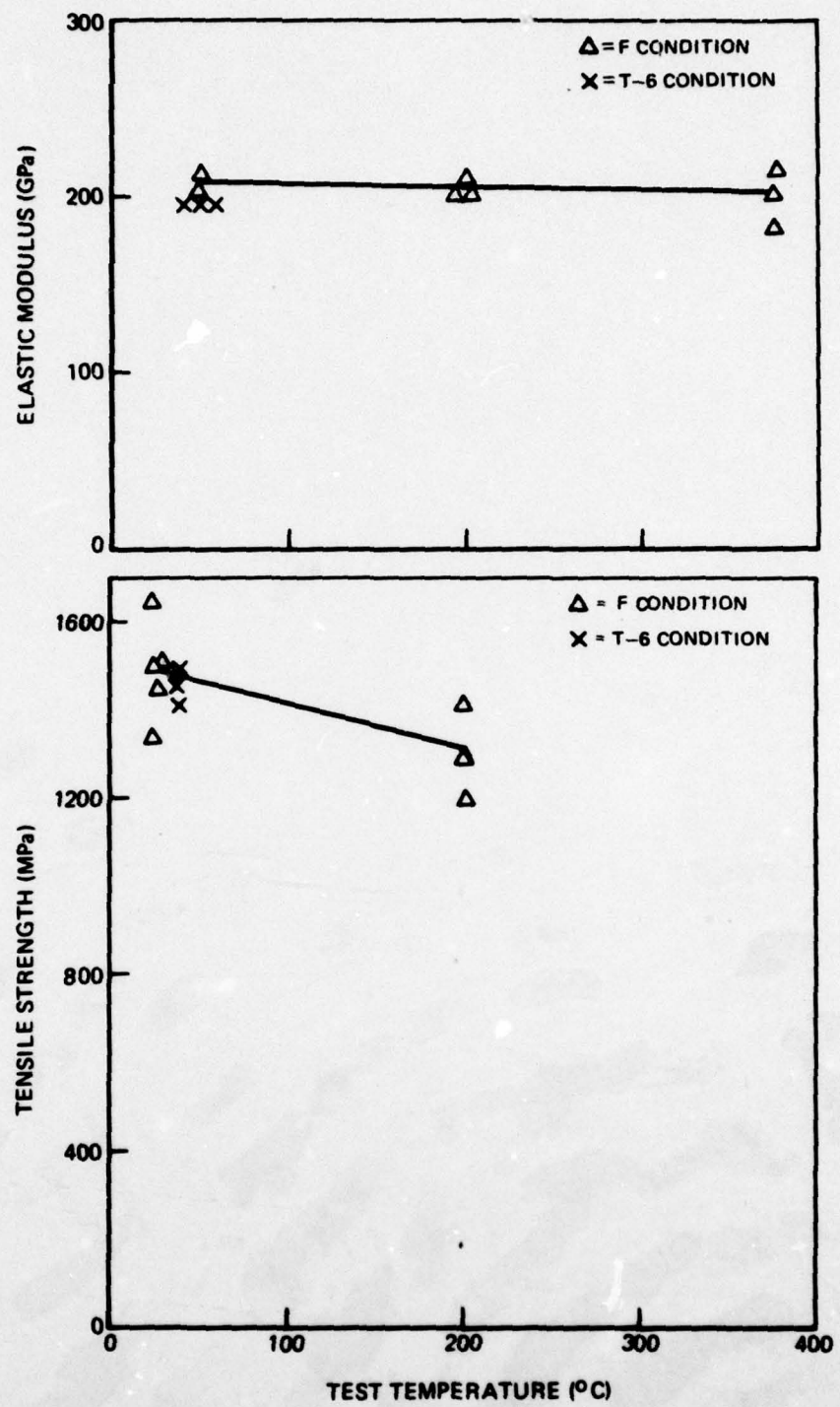


FIG. 6 AXIAL TENSILE STRENGTH AND ELASTIC MODULUS OF SIC REINFORCED ALUMINUM

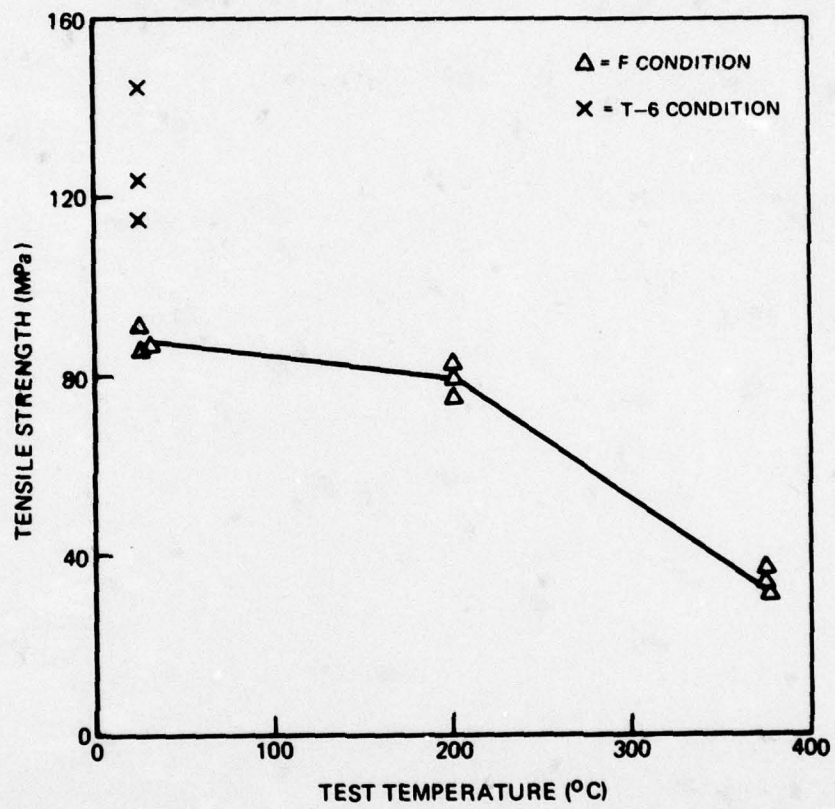


FIG. 7 TRANSVERSE TENSILE STRENGTH OF SC REINFORCED ALUMINUM

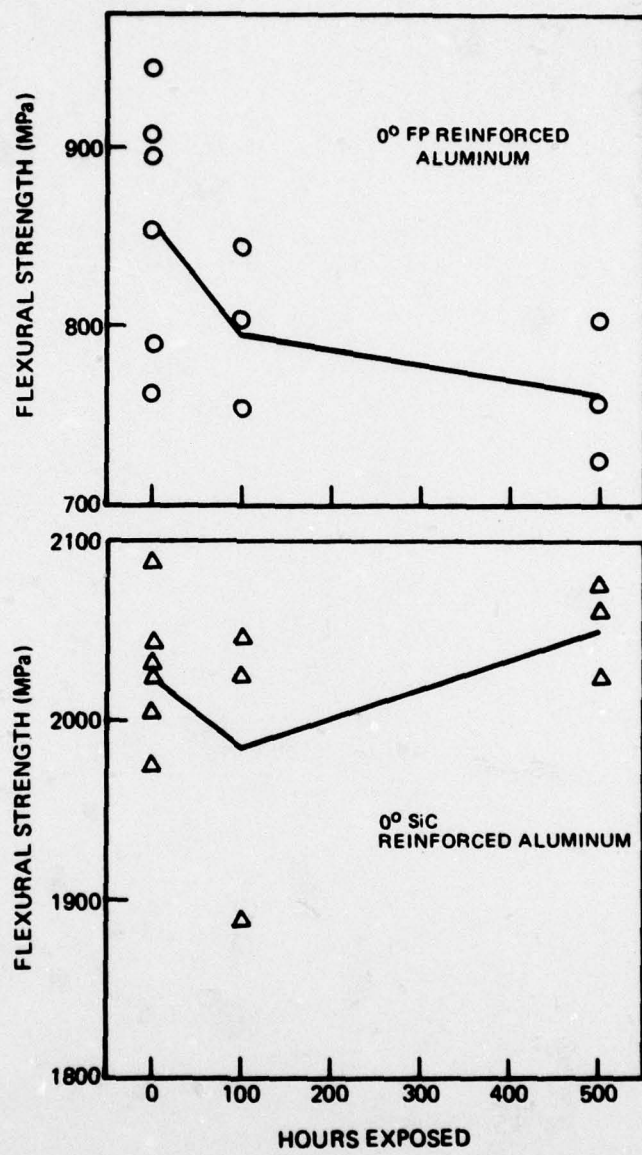


FIG. 8 RETENTION OF COMPOSITE LONGITUDINAL FLEXURAL STRENGTH AFTER EXPOSURE IN AIR AT 370°C

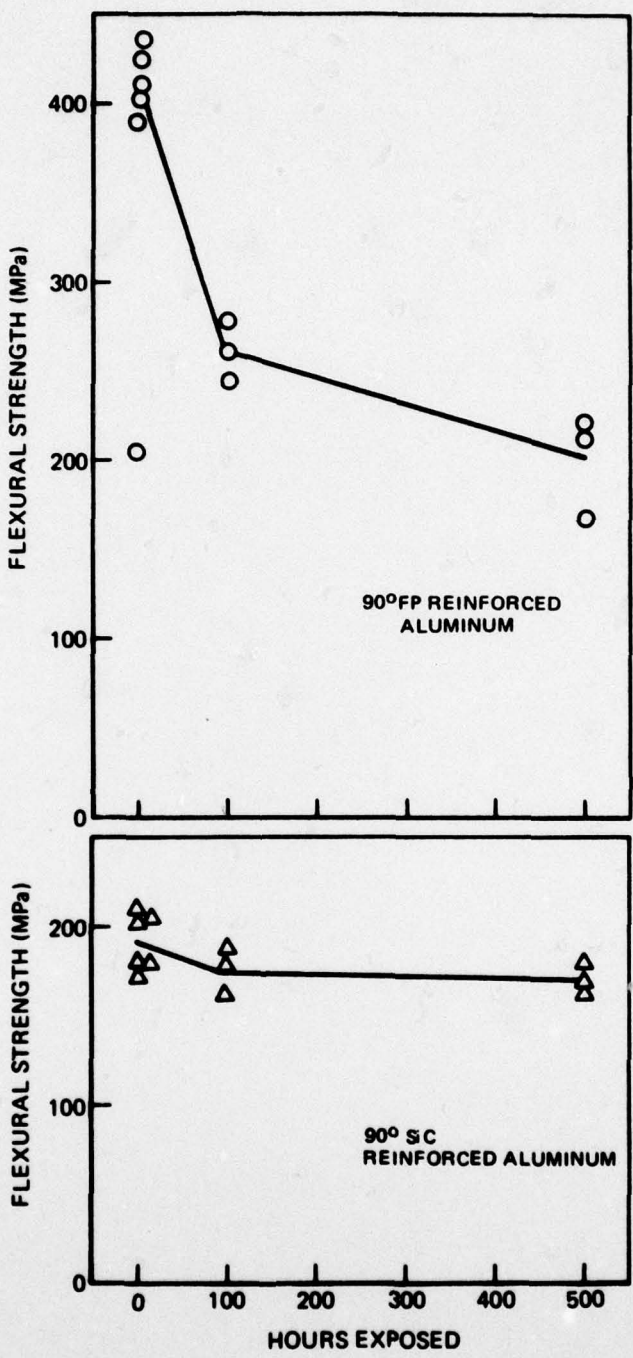


FIG. 9 RETENTION OF COMPOSITE TRANSVERSE FLEXURAL STRENGTH AFTER EXPOSURE IN AIR AT 370°C

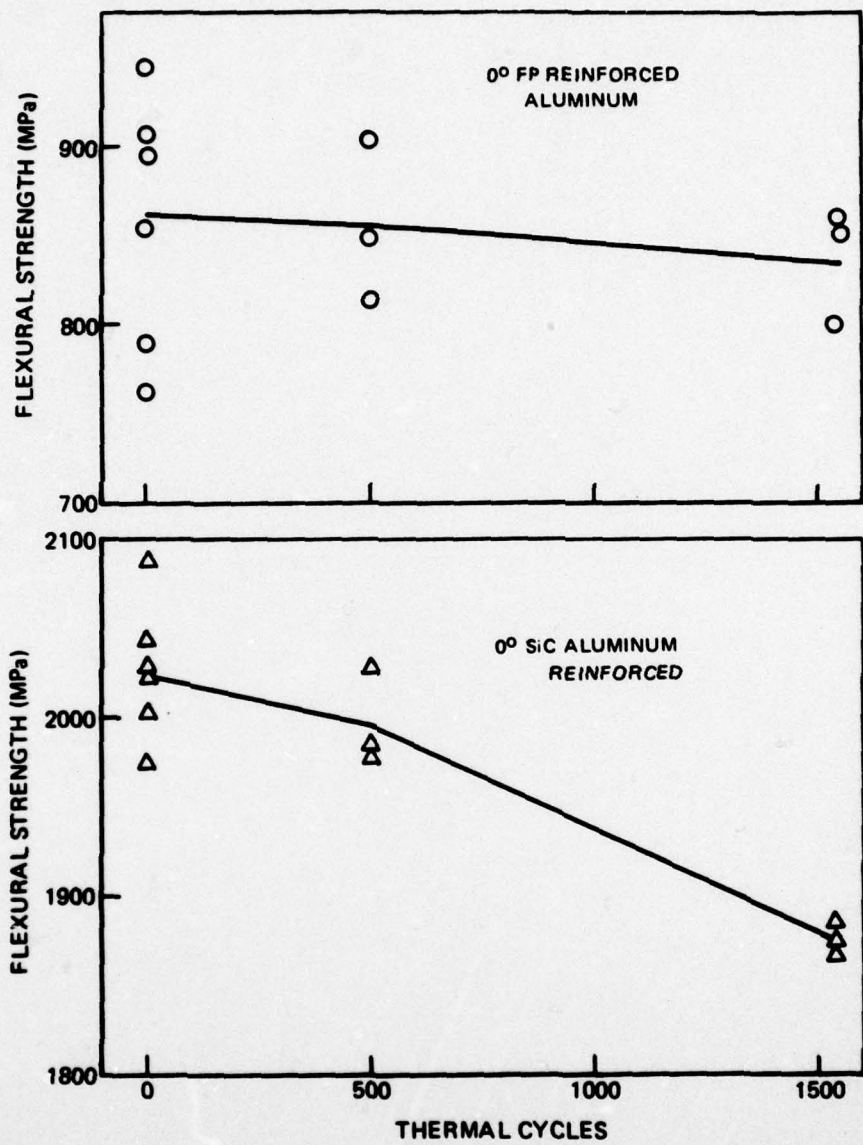


FIG. 10 RETENTION OF COMPOSITE LONGITUDINAL FLEXURAL STRENGTH
AFTER THERMAL CYCLING IN AIR BETWEEN 370°C AND 25°C

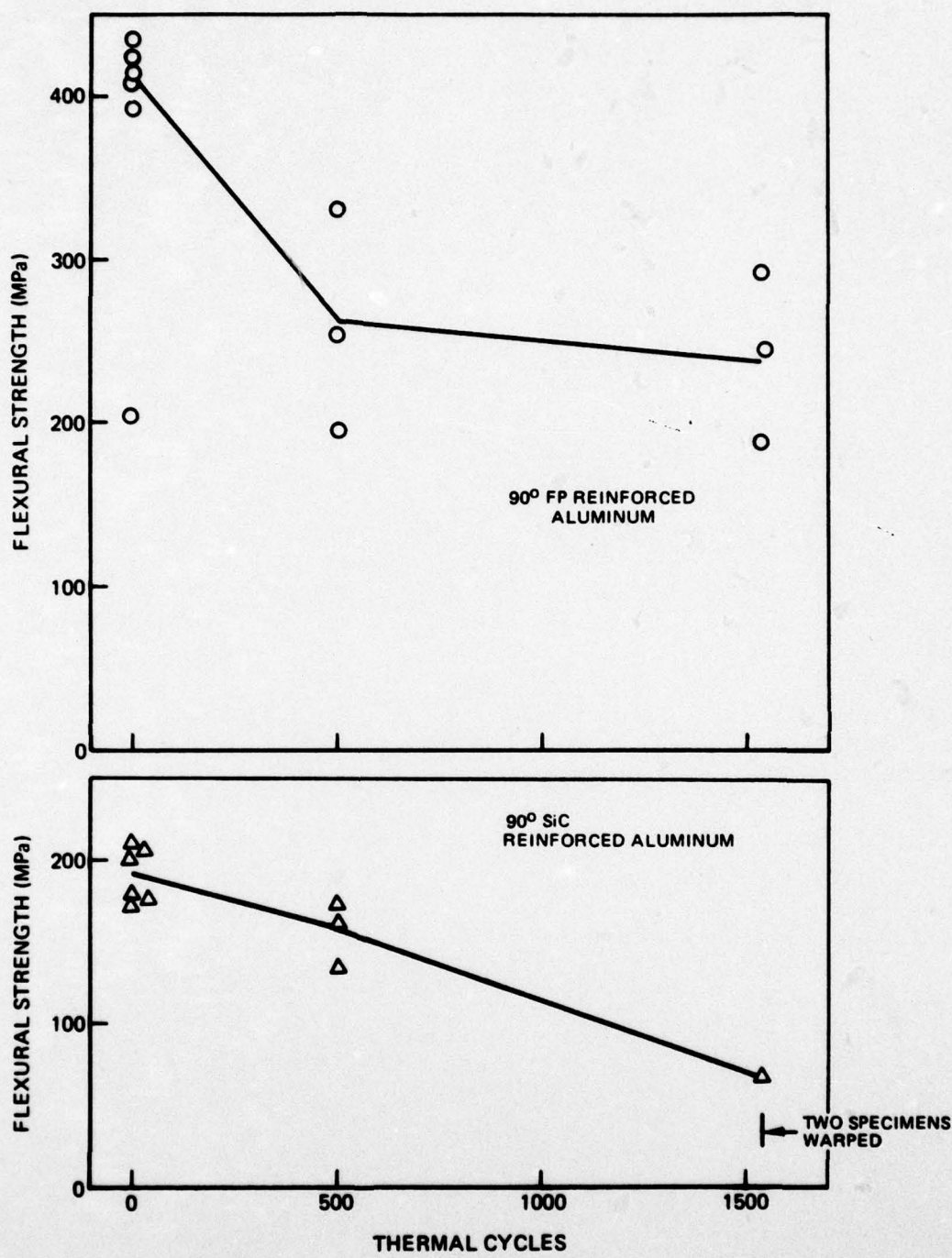


FIG. 11 RETENTION OF COMPOSITE TRANSVERSE FLEXURAL STRENGTH AFTER THERMAL CYCLING IN AIR BETWEEN 370°C AND 25°C

R79-9112245-6

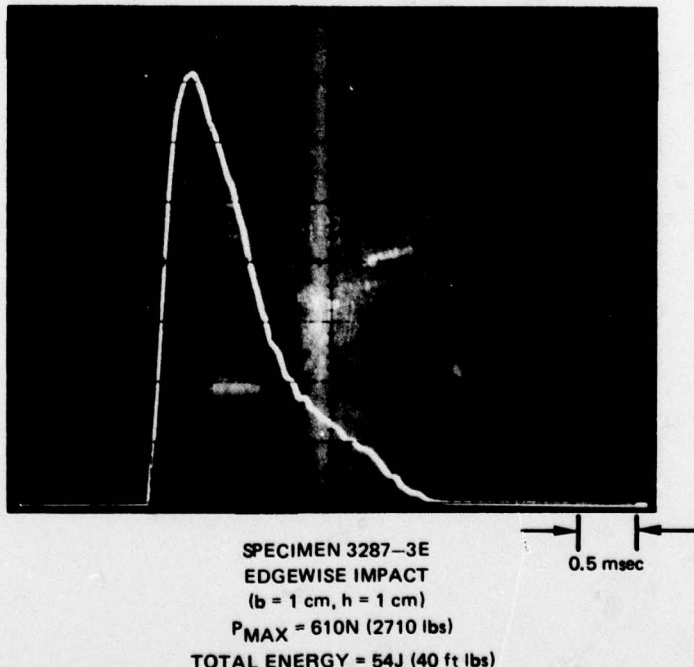
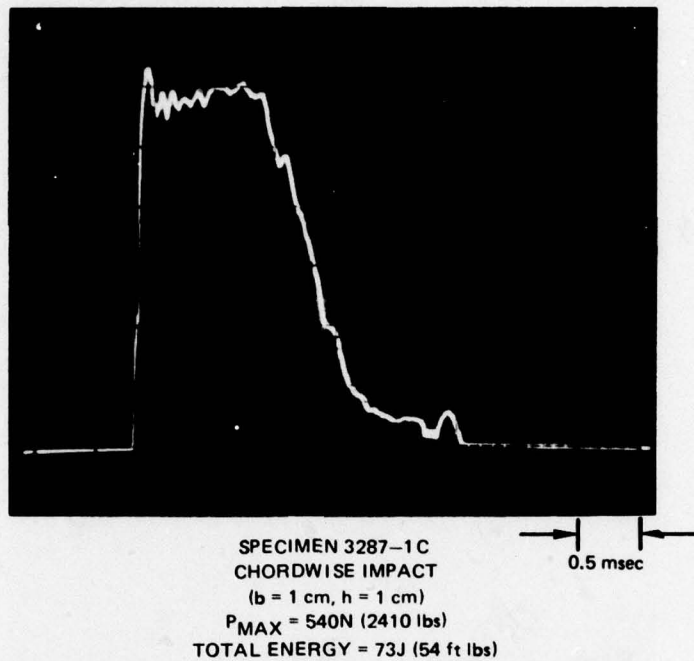
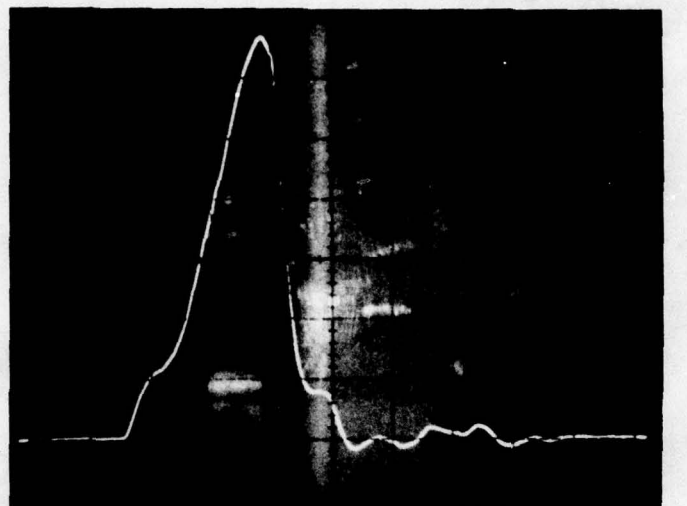
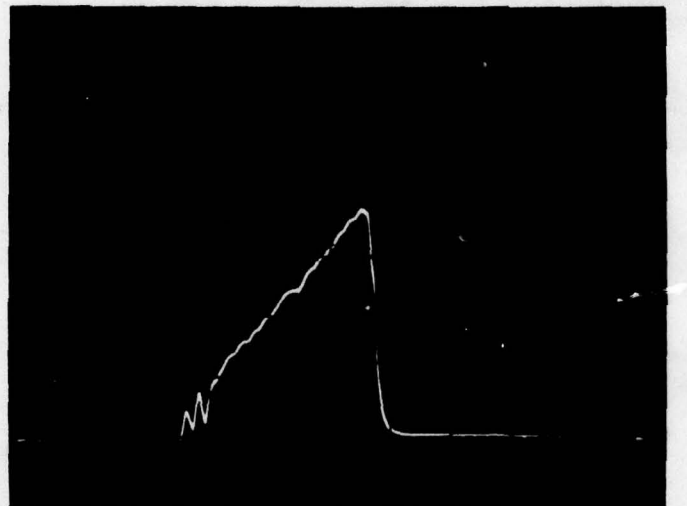


FIG. 12 INSTRUMENTED IMPACT TRACES FOR UNNOTCHED SiC REINFORCED ALUMINUM



SPECIMEN FP/Al-1
(b = 1 cm, h = 1 cm)
 $P_{MAX} \approx 619N$ (2755 lbs)
TOTAL ENERGY = 2.53J (1.87 ft lbs)

0.05 msec



SPECIMEN FP/Al-3
(b = 1 cm, h = 0.5 cm)
 $P_{MAX} = 140N$ (625 lbs)
TOTAL ENERGY = 0.76J (0.56 ft lbs)

0.1 msec

FIG. 13 INSTRUMENTED IMPACT TRACES FOR
UNNOTCHED FP-REINFORCED ALUMINUM

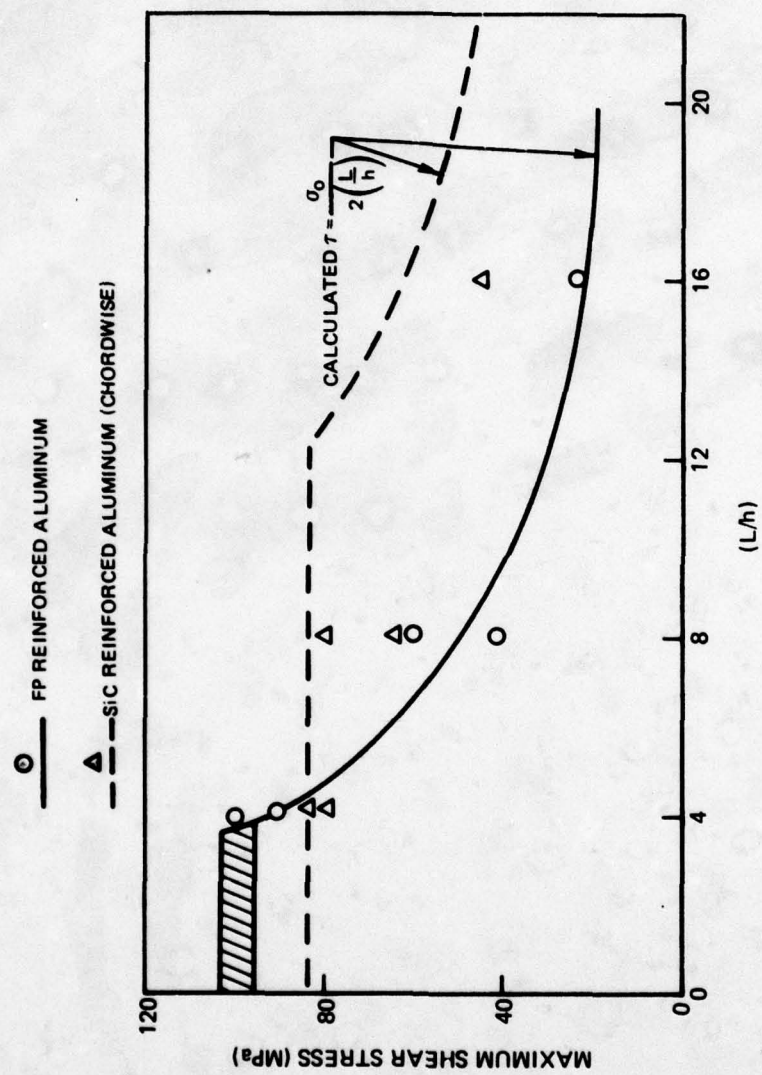


FIG. 14 SHEAR INTERACTION DIAGRAM

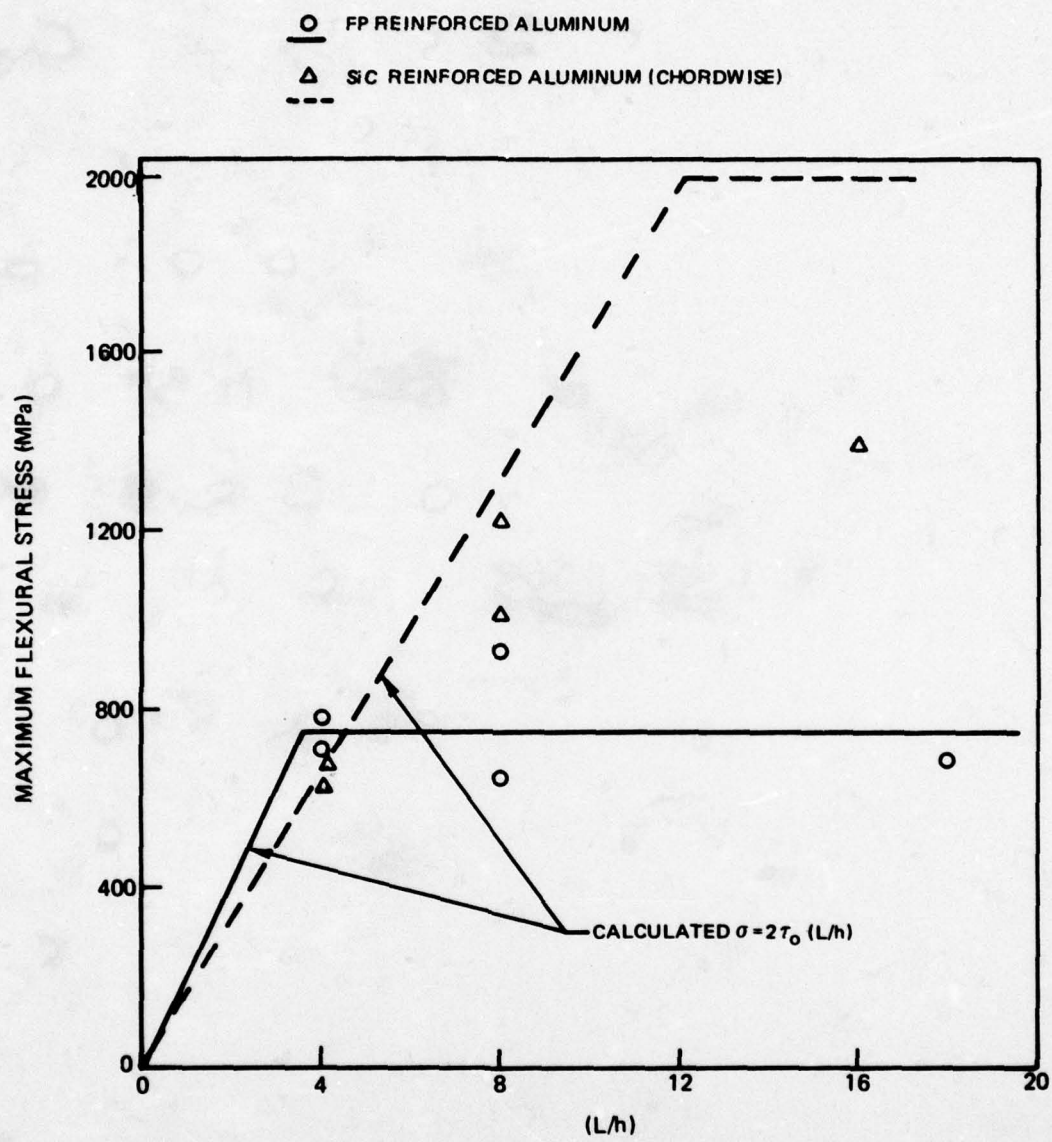


FIG. 15 FLEXURAL INTERACTION DIAGRAM

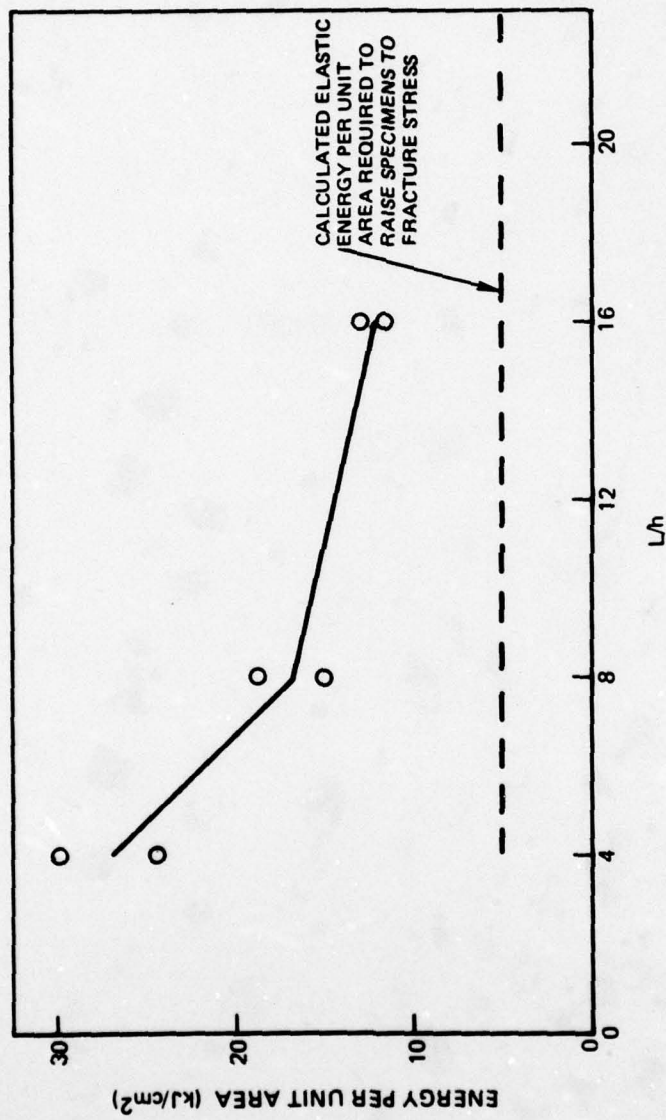


FIG. 16 ENERGY DISSIPATED IN FRACTURING FP REINFORCED ALUMINUM

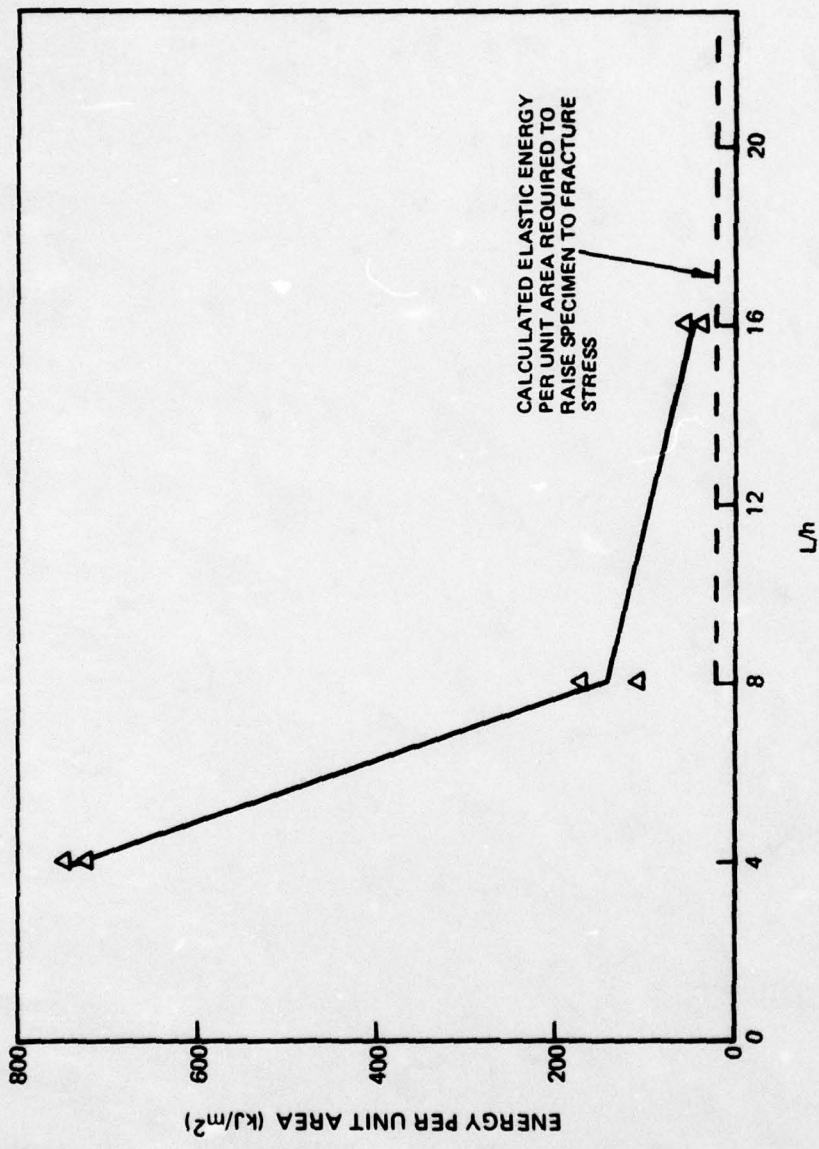


FIG. 17 ENERGY DISSIPATED IN FRACTURING SIC REINFORCED ALUMINUM (CHORDWISE)